Search Method for Gravitational Wave Transients Associated with the SGR 1806-20 Giant Flare

ABSTRACT

We describe a method for searching for transient gravitational waves associated with the SGR 1806-20 giant flare of 27 December 2004 using data collected by the LIGO 4 km detector located at Hanford, WA. We create an excess power time series from a time-frequency tiling by projecting elements in the frequency band of interest onto the time axis. This time series is calibrated with injections of known strength. An upper limit estimate can then be obtained by selecting the loudest event in the on-source region. Validations for the search and estimated sensitivity, obtained by performing the search on realistic simulated LIGO data, are presented.

Peter Kalmus, Rubab Khan, Luca Matone, Szabolcs Márka
Columbia University Experimental Gravity Group

1. An Extraordinary Event

On 27 December 2004, SGR 1806-20, a 'Soft Gamma Repeater' located 6-15 kpc away [1, 2], emitted the brightest transient ever observed [1, 6, 8, 11, 15].

This giant flare consisted of a short gamma-ray burst lasting ~0.2 s with isotropic energy of $2x10^{46}$ erg [1, 11] (or $\sim 1x10^{-8}$ $M_{sun}c^2$, as much as the sun radiates in a quarter million years), followed by a ~6 minute tail modulated at the star's rotation period of 7.56 s [6, 11, 15]. In addition there was a ~1 s precursor 142 s before the main flare, evidence of a ~1 hour X-ray afterglow [9], and a radio nebula expanding with a velocity of 0.3 c [5, 14].

During the event the LIGO 4 km detector at Hanford was operating under *Astrowatch*, an initiative for collecting data during commissioning periods [12], making a search for associated gravitational waves possible.

2. The Magnetar Model

According to the widely-accepted magnetar model, SGRs are neutron stars with magnetic fields of $\sim 1x10^{15}$ G, the strongest in the Universe and some 100 to 1000 times stronger than typical radio pulsars [4, 6, 16].

SGR bursts are explained by interaction of the magnetic field and the solid crust of the star, leading to bending and stretching of the crust, and occasionally catastrophic crustal cracking resulting in a giant flare [1, 4, 16]. Possible crustal reconfiguration during giant flares makes these events potential GW emitters in the ~kHz regime [3, 7].

3. Light Curve from the Event

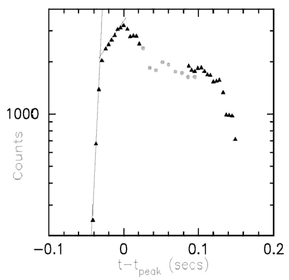

The light curve indicates timescales for the hard short burst event. The shortest timescale, ~1 ms, is set by the initial rise. The longest, ~100 ms, is set by the duration of the burst. This timescale, multiplied by a factor of 10, sets our on-source region of ±1 s around the start of the burst (the 'trigger'). Also, some models predict excitation of neutron star toroidal modes damped by gravitational waves on a timescale of ~1s [3]. (Fig. 2 from [13].)

4. The Search Strategy

We describe a single detector excess power search. We produce a time-frequency tiling from the data stream, each tile denoting significance relative to a background distribution of tiles at neighboring times and at the same frequency. This tiling is projected to the time axis to create a 1-dimensional significance time series.

If no element of this time series is larger than a predetermined false alarm threshold of 1 event in 10 years, we set upper limits.

The significance time series is calibrated via signals of known strength injected into the raw off-source data. Since the GW burst signature is unknown, we choose white noise bursts and sine-Gaussians with durations set by light curve timescales. White noise burst bandwidths are set by the shape of the detector sensitivity curve. An upper limit or sensitivity estimate can then be set from the loudest element in the on-source region. On-source and off-source regions are processed identically.

5. The Search Algorithm

Data Conditioning

Raw data is passed through digital bandpass and notch filters. The passband is ~60 to ~2000 Hz, implemented as a 12th order Butterworth with 2nd order sections. The notch filter is an aggregate of digital band-stop filters designed to remove 60 Hz and its harmonics, 'violin' modes of the test mass suspensions, calibration lines, and other lines of unknown origin. Data is passed backwards and forwards through the filter, ensuring no net phase change.

Calibration

We first choose a calibration signal flavor. We calibrate the band plot with signals of known and varying strength injected into the raw data. The strength of many injections are plotted against detected amplitudes, and the fit is used to determine a conversion from detected amplitude to injection-equivalent root-sum-square strain (h_{rss}). A one-sided 90% confidence belt can also be estimated.

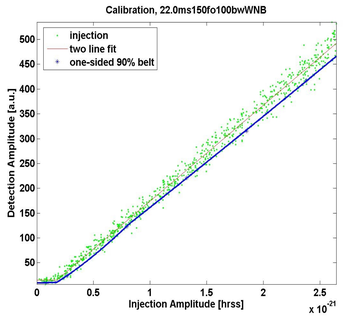

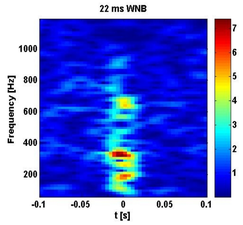

Left: Significancegram of an example white noise burst. Above: Example calibration curve made from simulated data. Red line is best fit, blue line is interpolated one-sided 90% confidence belt.

Creation of Tiling and Band Plot

Conditioned data is transformed into a spectrogram, which is a linear time-frequency tiling. We take the complex magnitude of the resulting matrix. We fit every frequency bin to a Weibull distribution after removing outliers, and for each tile in the bin subtract the mean and divide by the standard deviation; tiles now represent significance relative to a background distribution of other tiles at the same frequency but different times. We refer to this object as a 'significancegram'. Finally we choose tiles in a specified frequency band and sum them to obtain a projection onto the time axis. We refer to this as a 'band plot.'

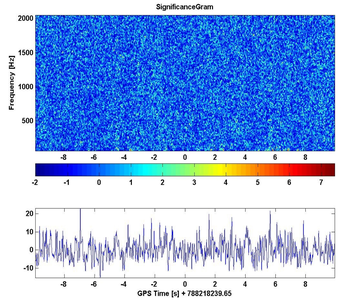

Above: Example significancegram and bandplot made from simulated data.

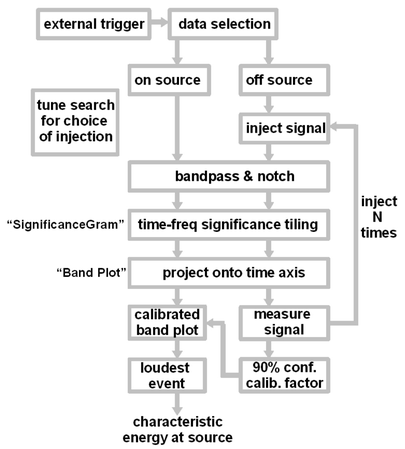

Tuning

The search relies on certain parameters, which can be chosen via tuning. These tuneable parameters are **fourier transform length** and **time overlap** and - for sine-Gaussian searches only - **search bandwidth**. The tuning algorithm searches this parameter space for the set producing optimal sensitivity.

6. Characterization and Validation

Hardware Injections

The search was tested on 14 sets of 235 Hz and 914 Hz Q 9 sine-Gaussians of 5 different amplitudes injected by the test mass coil drive into data in the fourth science run. Agreement between injected h_{rss} and recovered h_{rss} is ~5% or better for each group of injections.

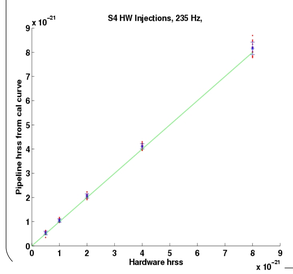

Software Injections

The search was tested repeatedly on data containing a randomly placed injection of known strength. Histograms of recovered h_{rss} values were checked for symmetry, spread and recovery of mean value. These injections are recovered to the ~1 percent level.

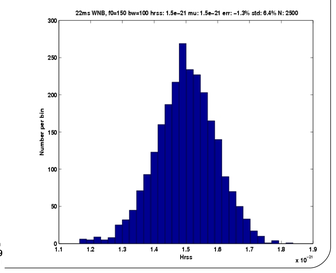

7. Estimated Sensitivity From Simulated Data

Simulated Noise

To create simulated noise, a segment of LIGO noise is taken as a model. The individual data samples are randomly shuffled. The amplitude spectral density of the result is then matched to the LIGO noise bin by bin in frequency space, and the resulting series is inverse transformed back to the time domain. The result is simulated noise with histogram and spectrum matching LIGO noise, but with increased entropy.

Sensitivity Estimates

Estimated sensitivities for 6 white noise bursts and 12 sine-Gaussians are plotted at right above a calibrated simulated noise curve. We take the loudest event in the 90% belt calibrated significance time series in 2s of **simulated** noise, at a location which corresponds to the on-source region, for an optimally located source emitting in the detectable polarization state. The loudest event over many runs on different simulated data has a standard deviation of ~20%. Error in calibration of the interferometer, which also affects the simulated data, is ~20%.

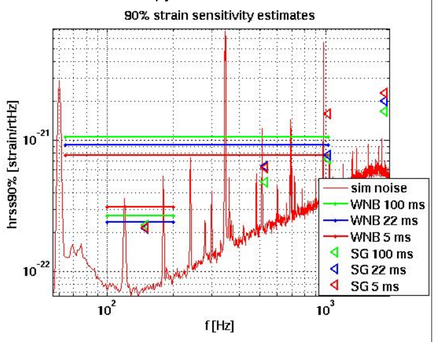

Astrophysical Interpretation

Strain sensitivites can be cast into characteristic gravitational wave emission energies at the source, for the simple model of isotropic emission and energy divided equally between polarizations, via

$$E_{GW} = 4\pi R^2 \frac{c^3}{16\pi G} \int_{-\infty}^{\infty} \left(\dot{h}_+\right)^2 + \left(\dot{h}_\times\right)^2 dt.$$

which can be derived from formulas in [10]. Here R is distance to the source, which we take as 10 kpc, and we assume the integral yields identical values for each polarization. The broadband strain sensitivity for 100 Hz wide white noise bursts with durations ranging from 5 ms to 100 ms, $<4x10^{-22}$ $Hz^{-1/2}$, corresponds to characteristic energy of $1x10^{-7}$ $M_{sun}c^2$ or less (the value depends on the injection type). The sine-Gaussian strain sensitivity at ~1 kHz ($<2x10^{-21}$ $Hz^{-1/2}$) corresponds to a characteristic energy of $1x10^{-4}M_{sun}c^2$.

1.Boggs, S.E. et al., astro-ph/0611318
2.Cameron, P. et al., Nature 434, 1112 (2005.
3.de Freitas Pacheco, J.A., Astron. Astrophys. 336, 397 (1998).
4.Duncan, R.C. and Thompson, C., Astrophysical Journal, Letters, 392, L9 (1992).
5.Gaensler, B.M. et al., Nature 434, 1104 (2005).
6.Hurley, K. et al., Nature 434, 1098 (2005).
7.Ioka, K. MNRAS 327, 639 (2001).
8.Mazets, E.P. et al., astro-ph/0502541.
9.Mereghetti, S. et al., Astrophysical Journal 624, L105 (2005.
10.Misner , Thorne and Wheeler, *Gravitation* (1973).
11.Palmer, D. M. et al., Nature 434, 1107 (2005).
12.Raab, F., LIGO internal document G050122-00-W.
13.Schwartz, S.J. et al., Astrophysical Journal, 627, L129 (2005).
14.Taylor, G.B. and Granot, J., MPLA 21, 2171 (2006).
15.Terasawa, T. et al., Nature 434, 1110 (2005).
16.Thompson, C. and Duncan, R.C. , MNRAS 275, 255 (1995).

The authors are grateful for the support of the United States National Science Foundation under cooperative agreement PHY-04-57528 and Columbia University in the City of New York. We are grateful to the LIGO collaboration for their support. We are indebted to many of our colleagues for frequent and fruitful discussion. The authors gratefully acknowledge the support of the United States National Science Foundation for the construction and operation of the LIGO Laboratory and the Particle Physics and Astronomy Research Council of the United Kingdom, the Max-Planck-Society and the State of Niedersachsen/Germany for support of the construction and operation of the GEO600 detector. The authors also gratefully acknowledge the support of the research by these agencies and by the Australian Research Council, the Natural Sciences and Engineering Research Council of Canada, the Council of Scientific and Industrial Research of India, the Department of Science and Technology of India, the Spanish Ministerio de Educacion y Ciencia, The National Aeronautics and Space Administration, the John Simon Guggenheim Foundation, the Alexander von Humboldt Foundation, the Leverhulme Trust, the David and Lucile Packard Foundation, the Research Corporation, and the Alfred P. Sloan Foundation.